INTERNATIONAL JOURNAL OF QUANTUM CHEMISTRY, VOL. XXXIX, 93–113 (1991)

Excited and Ionized States of RuO_4 and OsO_4 Studied by SAC and SAC-CI Theories

H. NAKATSUJI* AND S. SAITO†

Division of Molecular Engineering, Graduate School of Engineering, Kyoto University, Kyoto 606, Japan

Abstract

The excitation and ionization spectra of RuO_4 and OsO_4 are studied theoretically by the symmetry-adapted cluster (SAC) and SAC-CI theories. This is the attempt to assign whole of the spectra by ab initio claculations including electron correlations. In the ground state, electron correlations work to reduce the polarity of the M—O bond overestimated in the Hartree–Fock calculation. The Os—O bond is stronger than is the Ru—O bond, which is reflected in the differences of the excitation and ionization spectra of RuO_4 and OsO_4. The excitation energies of the experimental spectra are well reproduced by the SAC-CI theory, though the calculated intensities of some peaks are very small in comparison with the experiments. The outer-valence ionization spectra calculated by the SAC-CI theory agree well with the experimental photoelectron spectra. Some shake-up peaks that are accompanied with an electron-transfers from oxygen to metal are also calculated.

1. Introduction

It is generally recognized that electron correlations are important for adequate descriptions of excited states. We have developed cluster expansion-based theories, called symmetry-adapted cluster (SAC) [1] and SAC-CI theories [2], for the studies of electron correlations in ground, excited, ionized, and electron-attached states.

Transition-metal complexes are characterized by a variety of absorption spectra in visible and uv regions. Much experimental data have been accumulated for electronic spectra and photoelectron spectra. However, theoretical studies on the excited and ionized states of transition-metal complexes are still very limited. This is probably because transition-metal complexes are sometimes too large for accurate and reliable calculations for ground, excited and ionized states including electron correlations. For example, for MnO_4^- which is one of the most studied complexes, there is only one SDCI calculation [3] though five ab initio Hartree–Fock (HF) calculations [4] and several $x\alpha$ studies [5] have been reported. On the other hand, the SAC/SAC-CI theory is very suitable for the studies of excited, ionized, and anion states because of the several theoretical reasons [2, 6]. It seems to be more efficient than is an ordinary CI method.

* Present address: Department of Synthetic Chemistry, Faculty of Engineering, Kyoto University, Kyoto 606, Japan.

† Present address: Institute for Molecular Science, Okazaki 444, Japan.

 CCC 0020-7608/91/010093-21$04.00

In this article, we report the results of the applications of the SAC and SAC-CI theories to the ground, excited, and ionized states of RuO_4 and OsO_4. The excitation spectra of these two complexes are interesting. They are observed in a wide energy range of 3–11 eV for RuO_4 and 4–11 eV for OsO_4 [7]. The first six peaks in the lower-energy region have been assigned by the DVM-Xα method [8] and the SCF-Xα method [9], but no theoretical assignments have been made for the higher energy peaks. We are interested in the natures of the metal d–d transitions and the Rydberg transitions of these complexes.

The ionization spectra of these complexes are also interesting. They are observed by the ultraviolet photoelectron spectroscopy (UPS) in a gas phase [10]. In the higher-energy region, the experimental spectra are very broad and the presence of the shake-up satellites is considered. The shake-up ionization is a two-electron process and shows a breakdown of the one particle HF model. Electron correlations play an essential role in the appearance of the shake-up peaks.

2. Calculational Details

Molecular geometries are fixed, in this calculation, to the regular tetrahedron, and the metal-oxygen bond lengths are taken from the experimental values, 1.706 and 1.711 Å for the Ru—O and Os—O bonds [11], respectively.

The relativistic effective core potential method [12] is used for the central metals, Ru and Os, and the (3*s*3*p*4*d*)/[3*s*2*p*3*d*] and (3*s*3*p*3*d*)/[3*s*2*p*3*d*] CGTOs for the *ns*, *np*, and $(n-1)d$ orbitals of Ru and Os, respectively [12]. The basis set of oxygen is the (63/5) GTOs [13] contracted to [3*s*2*p*], plus two *s*-type functions (α = 0.0608, 0.0240) [14] and a *p*-type function (α = 0.028) [14] for the Rydberg orbitals. The HF MOs of the ground state are calculated with the program GAMESS [15].

The electron correlations in the ground state are taken into account by the SAC theory [1]. The HF MOs are used as the reference orbitals. The excited and ionized states are calculated by the SAC-CI theory [2]. The calculations are carried out with use of the program SAC85 [16].

The active space in the SAC/SAC-CI calculations consists of 12 higher occupied orbitals and 38 lower unoccupied orbitals. All single-excitation operators are included without selection. The double-excitation operators in the linked term are selected by the second-order perturbation method [17]. For the ground state, the double-excitation operators whose perturbation energy with the HF configuration is larger than 3×10^{-5} a.u. are included. For the excited states, the threshold of 1×10^{-4} a.u. is used with respect to the main configurations of the excited states. For the ionized states, all the double-excitation operators are included for studying the shake-up peaks. In the SAC and SAC-CI theories, the triple and quadruple excitations are considered in the unlinked terms as the products of the lower excitations. The selections are performed by the method described previously [17]. Table I shows the dimensions of the SAC/SAC-CI calculations for the ground, excited, and ionized states of RuO_4 and OsO_4. Because of the merit of the present theories, the dimensions are small in comparison with those of the ordinary CI of comparable accuracy.

TABLE I. Dimensions of the SAC and SAC-CI calculations.

State	Symmetry (C_{2v})	RuO_4	OsO_4	Without selection
Ground	$^1A_1$	2124	2380	(26491)
Excited	$^1A_1$	6945	8471	(26491)
	$^1A_2$	7081	8514	(25950)
	$^1B_1$	7412	8217	(26106)
Ionized	$^2A_1$	1396	1396	(1396)
	$^2A_2$	1346	1346	(1346)
	$^2B_1$	1371	1371	(1371)

3. Results and Discussions

3.1. Ground States

The HF energies and the correlation energies of RuO_4 and OsO_4 are given in Table II. The HF configuration of RuO_4 is written as

$$(\text{core})^{16}(1e)^4(1t_2)^6(2t_2)^6(1a_1)^2(1t_1)^6\ (2e)^0(3t_2)^0(2a_1)^0(4t_2)^0$$
$$\text{M}+\text{OM}+\text{O}\ \ \text{O}\quad \text{M}\quad \text{O}\quad \text{M}-\text{OM}-\text{O}\ \ \text{M}\quad \text{O(R)}$$

where M and O denote metal and oxygen AOs, respectively, and M ± O means bonding and antibonding combinations. O(R) refers to the Rydberg orbital of oxygen. The lowest two valence orbitals, $1e$ and $1t_2$, are the bonding MOs between d(M) and $2p$(O). The highest occupied orbitals $1t_1$ are the nonbonding MOs of the $2p$(O) character. The virtual orbitals, $2e$ and $3t_2$, are the antibonding MOs between d(M) and $2p$(O). The natures of these MOs are the same as those of MnO_4^-, which is valence iso-electronic structure with RuO_4 and OsO_4.

The HF configuration of OsO_4 is

$$(\text{core})^{16}(1e)^4(1t_2)^6(1a_1)^2(2t_2)^6(1t_1)^6\ (2e)^0(3t_2)^0(2a_1)^0(4t_2)^0$$
$$\text{M}+\text{OM}+\text{O}\ \ \text{M}\quad \text{O}\quad \text{O}\quad \text{M}-\text{OM}-\text{O}\ \ \text{M}\quad \text{O(R)},$$

and the ordering of the $1a_1$ and $2t_2$ MOs is different from that of RuO_4. The MO natures of OsO_4 are almost the same as those of RuO_4.

It is well known that both RuO_4 and OsO_4 are oxidizing agents and RuO_4 is a stronger oxidizing agent than is OsO_4 as seen from the oxidation-reduction po-

TABLE II. Ground-state energies of RuO_4 and OsO_4 calculated by the Hartree-Fock and SAC methods (in a.u.).

Method	RuO_4	OsO_4
Hartree-Fock	−315.37754	−313.98366
SAC	−0.44360	−0.37086

The correlation energy is given for the SAC method.

tential. This is qualitatively explained as follows. In the orbital model, electron affinity is estimated from the orbital energy of the lowest unoccupied valence MO. In the present calculations, the LUMO energy of RuO_4 is -4.1 eV and that of OsO_4 is -2.9 eV, suggesting that RuO_4^- is more stable than is OsO_4^-. This indicates that RuO_4 is a stronger oxidizing agent than is OsO_4.

The net charges of RuO_4 and OsO_4 calculated by the HF and SAC methods are given in Table III. The HF solution shows more strongly ionic in the M—O bond than does the SAC solution. The ionic character of the M—O bond is somewhat relaxed by the inclusion of electron correlations. Table IV shows the occupation numbers of the natural orbitals. As expected from Table III, the electron correlations work to reduce the occupations from the oxygen localized MOs ($2t_2$ and $1t_1$) and to increase them in the delocalized M − O ($2e$ and $3t_2$) MOs. The natural orbital occupancies of OsO_4 are slightly more rapidly convergent than those of RuO_4. In the case of FeO and RuO, Krauss and Stevens have shown that the occupancies of RuO converge more rapidly than do those of FeO [18].

Now we investigate the nature of the M—O bonds. In tetrahedral complexes, the central metal forms d^3s hybridization using the s, d_{xy}, d_{yz}, and d_{xz} orbitals. This hybridization is easy when $(n-1)d$–ns level splitting is small. Moreover, when the energy levels of these s and d AOs are close to the oxygen $2p$ level, the M—O bonds are strongly formed. Figure 1 shows the atomic-energy levels of Ru, Os, and oxygen. The energy level of the stable configuration $(4d)^7(5s)^1$ of the Ru atom is estimated by using its first ionization potential ($-\varepsilon 5s$) and the d–s level splitting is taken from the excitation energy to $(4d)^6(5s)^2$ and $(4d)^8$ [19]. The diagram of the Os atom is similarly made [19]. The $(n-1)d$–ns level splittings are about 0.953–1.172 eV and 0.703 eV for Ru and Os, respectively; i.e., the d^3s hybridization is expected to be formed more easily in OsO_4 than in RuO_4. Furthermore, the energy levels of the valence s and d orbitals of the Os atom are closer to the oxygen $2p$ level than are those in the Ru atom. We therefore conclude that the Os—O bond should be stronger than the Ru—O bond. We have confirmed in the calculational results that the bond-order matrices give the same result. The experimental force constants for the Ru—O and Os—O stretching vibrations in the MO_4 complexes are 6.96 and 8.29 mdyn/Å [20], respectively. Thus, the qualitative prediction on the strength of the M—O bond based on the atomic-energy levels is confirmed. The arguments on metal chemical shifts based on the atomic-energy levels are reported previously [21]. We will see in the following sections that this difference in the strength of the M—O bonds is reflected in the differences of the excitation and ionization spectra of RuO_4 and OsO_4.

3.2. Excited States of RuO_4

Figure 2 shows the electronic spectra of RuO_4; the upper one is a spectrum observed by Foster et al. [7], and the lower one, the theoretical spectrum calculated in this study. Table V gives the numerical values for the excitation energies, oscillator strengths, and the second moments of the excited states. We divide the

TABLE III. Population analyses and net atomic charges on M and O of RuO_4 and OsO_4.

	RuO_4							OsO_4						
	Ru				O			Os				O		
State (method)	*s*	*p*	*d*	Charge	*s*	*p*	Charge	*s*	*p*	*d*	Charge	*s*	*p*	Charge
Ground (HF)	0.368	0.370	5.533	+1.711	3.949	4.479	−0.428	0.579	0.467	5.460	+1.493	3.879	4.494	−0.373
Ground (SAC)	0.376	0.385	5.580	+1.441	3.943	4.418	−0.360	0.584	0.530	5.759	+1.128	3.872	4.411	−0.282
$1T_2$ (SAC-CI)	0.378	0.344	5.591	+1.337	3.398	4.396	−0.334	0.590	0.486	5.892	+1.033	3.869	4.389	−0.258

TABLE IV. Occupation number of the natural orbitals of the ground state of RuO_4 and OsO_4.

		SAC	
MO	Hartree-Fock	RuO_4	OsO_4
$1e$	4.0	3.96	3.96
$1t_2$	6.0	5.94	5.94
$2t_2$	6.0	5.91	5.92
$1a_1$	2.0	1.96	1.97
$1t_1$	6.0	5.90	5.89
$2e$	0.0	0.15	0.15
$3t_2$	0.0	0.16	0.14
$2a_1$	0.0	0.00	0.01
$4t_2$	0.0	0.02	0.02

whole spectra into three regions. Region A is from 3 to 7 eV, region B from 8 to 10 eV, and region C from 10 to 11 eV.

First we discuss region A. In the T_d symmetry, only the transitions to the T_2 states are symmetry allowed. The forbidden transition to the $1T_1$ state [$1t_1(2p(O)) \rightarrow 2e(M - O)$] is predicted at 2.70 eV by the present calculations, though it is not observed in the experimental spectrum. In MnO_4^-, the first transition is also assigned to the electronic forbidden transition, $1t_1(2p(O)) \rightarrow 2e(M - O)$ [3, 8]. The first observed band that has maximum at 3.22 eV

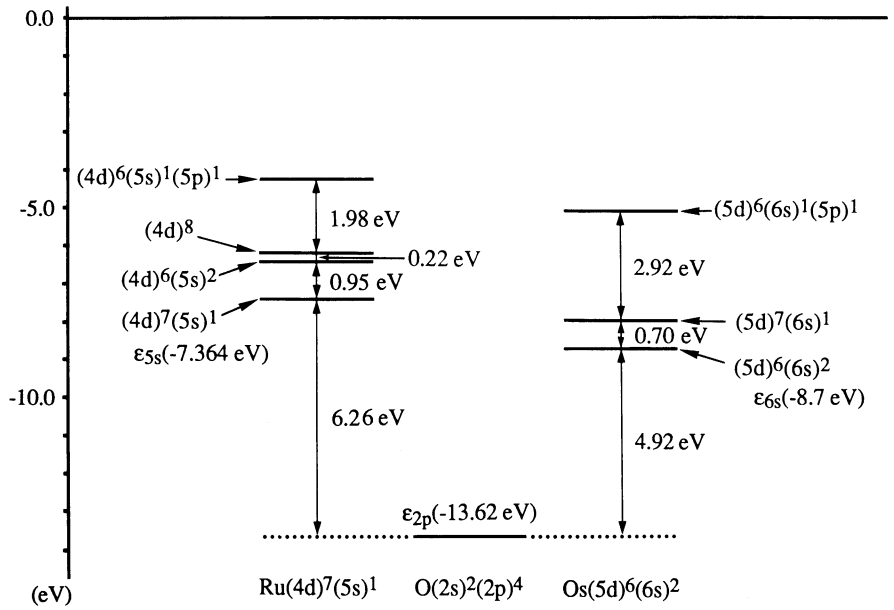

Figure 1. Atomic-energy levels of Ru, Os, and oxygen.

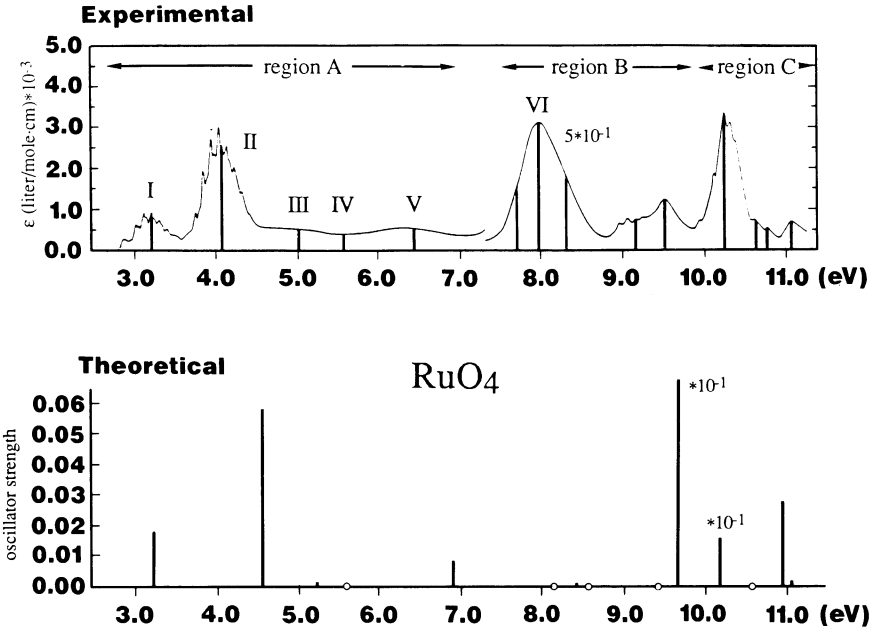

Figure 2. Experimental and theoretical electronic excitation spectra of RuO_4. Experimental spectra are cited from Ref. 7.

(26,000 cm^{-1}) is due to the electronic allowed transition to the $1T_2$ state [$1t_1(2p(O)) \rightarrow 2e(M - O)$]. We assign the strong band at 4.09 eV (33,000 cm^{-1}) to the allowed transition to the $2t_2$ state [$2t_2(2p(O)) \rightarrow 2e(M - O)$]. The present calculations show that the configurations, $1t_1 \rightarrow 2e$ and $2t_2 \rightarrow 2e$, strongly mix to each other. In the experimental spectrum, bands I and II show many vibrational structures, suggesting that the molecular geometry is not much changed by the transitions. This is because these excitations are from the nonbonding MOs to the weakly antibonding MOs as shown in the HF MO sequence. The third observed peak at 5.03 eV (40,600 cm^{-1}) is assigned to the $3T_2$ state [$1t_1(2p(O)) \rightarrow 3t_2(M - O)$]. Our assignments for the lower three transitions are the same as those of the DVM-Xα [8] and the SCF-Xα [9] calculations. Next, two peaks at 5.58 eV (45,000 cm^{-1}) and 6.45 eV (52,000 cm^{-1}) are assigned to the $3T_1$ state [$1t_1(2p(O)) \rightarrow 3t_2(M - O)$] and the $4T_2$ state [$2t_2(2p(O)) \rightarrow 3t_2(M - O)$], respectively. The DVM-Xα and the SCF-Xα calculations have assigned these two excitations to $2t_2 \rightarrow 3t_2$ and $1a_1(s(M)) \rightarrow 3t_2(M - O)$, respectively [8, 9]. For the fifth excitation, the $1a_1 \rightarrow 3t_2$ transition is the second largest configuration in the present calculations. Thus, in region A, the excitation energies and intensities calculated by the SAC-CI method are in good agreement with the experimental results. The transitions in this region are roughly characterized as the electron-transfer excitations from oxygen to metal.

Previous studies [8, 22] have argued that a small electron flow from M to O occurs along with the transition to the $1T_2$ states on MnO_4^-, though the main

configuration for this excitation is $1t_1 \rightarrow 2e$, which corresponds to the reverse electron transfer from O to M. They therefore concluded that the term, charge transfer, is misleading for this transition. Table III shows the results of the present calculations. Contrary to the previous results, the charges on the metal of RuO_4 and OsO_4 decrease by 0.104 and 0.095, respectively, by this excitation. Though the amount is much less than unity, the present calculations show that the electron transfer from O to M does occur in the $1T_2$ states. The present results shows that the d orbital population in the $1T_2$ state is larger by about 0.1 than in the ground state, whereas in the previous ones, the d orbital population in the $1T_2$ state was equal to or smaller than that in the ground state. Thus, the change in the d orbital population explains the above difference between the present and previous results [8, 22].

Next, we examine region B, 8–10 eV. The observed peaks in this region are more difficult in assignment than are those in region A. We tentatively assign the peaks as follows for the excitation energy, since in this region the calculated intensities poorly agree with the experimental ones: The observed peaks at 7.69 eV (62,000 cm^{-1}) and 8.00 eV (64,500 cm^{-1}) are assigned to the transitions to the $5T_1$ and $5T_2$ states, which are respectively, the forbidden and allowed elements of $1t_2(M + O) \rightarrow 2e(M - O)$. The peak at 8.31 eV (67,000 cm^{-1}) is attributed to the forbidden transition, $4E[1e\ (M + O) \rightarrow 2e(M - O)]$. The bands at 9.16 eV (74,000 cm^{-1}) and 9.55 eV (77,000 cm^{-1}) are assigned to the $6T_1$ state $[1t_1(2p(O)) \rightarrow 2a_1(s(M))]$ and the $6T_2$ state $[1t_2(M + O) \rightarrow 3t_2(M - O)]$, respectively. The $6T_1$ state has a large second moment and consists mostly of the diffuse s orbital of the central metal. The mixing of the Rydberg orbitals of oxygen is small. Band VI in the experimental spectrum given in Figure 2 has no vibrational structure. This fact suggests that the molecular structure of this excited state largely differs from that of the ground state. Our calculations show that the $5T_1$, $5T_1$, $4E$, and $6T_2$ states are the excitations from the metal-oxygen bonding orbitals to the antibonding orbitals. Consequently, a large change in the molecular geometry is expected in these excited states.

We consider that the effect of molecular vibration on the spectral intensity has to be examined in this region. The observed peak at 8.00 eV has a strong intensity, but the calculated intensity is fairly weak. Two origins may be considered for this intensity. One is the vibronic coupling. In the T_d symmetry, all the electronically forbidden transitions of the symmetries A_1, A_2, E, and T_1 become allowed by the coupling with the vibrations of the t_2 symmetry. The transition moment of the m-th state, $M_m(Q)$, which interacts with the k-th state through the vibronic coupling is given by

$$M_m(Q) = M_m^0 + \sum_k \langle \Psi_k^0(q) | \sum_i \sum_\sigma Z_\sigma \left(\frac{\partial \mathbf{R}_\sigma}{\partial Q_a} \right) \left(\frac{\mathbf{r}_{i\sigma}}{r_{i\sigma}^3} \right) | \Psi_m^0(q) \rangle \frac{Q_a M_k^0}{E_m^0 - E_k^0},$$

where M_m^0, $\Psi_m^0(q)$, and E_m^0 are, respectively, the transition moment, electronic wave function, and energy of the m-th state at the equilibrium nuclear configuration. Q_a denotes the normal coordinate of the irreducible representation a; $\mathbf{R}_\sigma$, the vector of the σ-th nucleus; and $\mathbf{r}_{i\sigma}$, the vector from the i-th electron to the

σ-th nucleus. In the present case, the theoretical energy difference between the $5T_2(1t_2 \rightarrow 2e)$ and $6T_2(1t_2 \rightarrow 3t_2)$ states is only 1.3 eV (1.6 eV in experiment) and the $6T_2$ has a considerably large strength, so that the transition to the $5T_2$ state may borrow a considerable amount of intensity from that to the $6T_2$ state. Another factor to be considered is the Jahn–Teller distortion of the states of degenerate symmetry. When the T_d symmetry is transformed into a lower symmetry on the basis of the Jahn–Teller effect, for example, to the D_{2d}, D_2, or C_{3v} symmetry, the T_1 state becomes allowed in the D_{2d} or D_2 symmetry and the E and T_1 states become allowed in the C_{3v} symmetry. Thus, the forbidden transitions of the E and T_1 symmetries in Table V may have some intensities through the vibronic interaction and/or the Jahn–Teller distortion.

Finally, we investigate the peaks in region C. The observed four peaks are assigned as follows: The strong observed peak at 10.29 eV (83,000 cm^{-1}) is attributed to the $7T_2$ state $[2t_2(2p(O)) \rightarrow 2a_1(s(M))]$. The next peak at 10.66 eV (86,000 cm^{-1}) probably corresponds to the $7T_1$ state $[1e(M + O) \rightarrow 3t_2(M - O)]$ from the energetic point of view. This excitation is the forbidden transition in the T_d symmetry but becomes allowed if the vibronic coupling and the Jahn–Teller effect are considered. The remaining peaks at 10.79 eV (87,000 cm^{-1}) and 11.10 eV (89,500 cm^{-1}) are assigned to the $8T_1$ state $[1t_1(2p(O)) \rightarrow 4t_2(3s(O))]$ and the $8T_2$ state $[1e(M + O) \rightarrow 3t_2(M - O)]$, respectively, based on the energy and strength of the spectrum. The peak observed at 10.79 eV is the first allowed Rydberg excitation within the ligands. Foster et al. [7] have considered that the Rydberg excitations of oxygen start from 7.69 eV. However, the present calculations show that the Rydberg excitations lie in about 11 eV in the RuO_4 spectrum. The present calculations thus show that the transitions in region C are from metal to metal, oxygen to metal, and the Rydberg excitations within the oxygen ligands.

The average discrepancy between the theoretical and experimental transition energies in all of the three regions A–C is only 0.21 eV.

3.3. Excited States of OsO_4

For the excited states of OsO_4 there has been no theoretical calculations. The observed spectrum of OsO_4 is also divided into three regions. The theoretical and experimental transition energies, the oscillator strengths, and the second moments of the excited states are summarized in Table VI. The experimental [7] and theoretical spectra are compared in Figure 3.

Region A, 4–8 eV, consists of the electron-transfer excitations from oxygen to metal. Five peaks are observed at 4.34 eV (35,000 cm^{-1}), 5.21 eV (42,000 cm^{-1}), 5.95 eV (48,000 cm^{-1}), 6.94 eV (56,000 cm^{-1}), and 7.94 eV (64,000 cm^{-1}). The assignments of these peaks are all the same as those for RuO_4; $1T_2$ state $[1t_1(2p(O)) \rightarrow 2e(M - O)]$, $2T_2$ state $[2t_2(2p(O)) \rightarrow 2e(M - O)]$, $3T_2$ state $[1t_1(2p(O)) \rightarrow 3t_2(M - O)]$, $3T_1$ state $[1t_1(2p(O)) \rightarrow 3t_2(M - O)]$, and $4T_2$ state $[2t_2(2p(O)) \rightarrow 3t_2(M - O)]$, respectively, in the increasing order of energy. The experimental and theoretical results show that the intensities of the OsO_4 spectra are stronger than those of RuO_4.

TABLE V. Excitation energies of RuO_4 (in eV).

State	Main configuration	SAC-CI			Experimental[a]			DVM-Xα[b]	SCF-Xα[c]
		Excitation energy	Oscillator strength	Second moment	Excitation energy	Strength	Band	Excitation energy	Excitation energy
Region A									
$1T_1$	$1t_1 \rightarrow 2e$ (O $\rightarrow$ M $-$ O)	2.70	Forbidden	141					
$1T_2$	$1t_1 \rightarrow 2e$ (O $\rightarrow$ M $-$ O)	3.22	$1.28 * 10^{-2}$	141	3.22	S	I	3.02	2.40
$2T_1$	$2t_2 \rightarrow 2e$ (O $\rightarrow$ M $-$ O)	3.51	Forbidden	141					
$1E$	$1a_1 \rightarrow 2e$ (M $\rightarrow$ M $-$ O)	4.10	Forbidden	141					
$2T_2$	$2t_2 \rightarrow 2e$ (O $\rightarrow$ M $-$ O)	4.55	$5.78 * 10^{-2}$	141	4.09	S	II	3.81	3.88
$2E$	$1t_1 \rightarrow 3t_2$ (O $\rightarrow$ M $-$ O)	5.05	Forbidden	141					
$3T_2$	$1t_1 \rightarrow 3t_2$ (O $\rightarrow$ M $-$ O)	5.23	$1.12 * 10^{-3}$	142	5.03	W	III	4.56	5.24
$3T_1$	$1t_1 \rightarrow 3t_2$ (O $\rightarrow$ M $-$ O)	5.60	Forbidden	141	5.58	W	IV	5.37[d]	5.74[d]
$1A_2$	$1t_1 \rightarrow 3t_2$ (O $\rightarrow$ M $-$ O)	5.78	Forbidden	141					
$1A_1$	$2t_2 \rightarrow 3t_2$ (O $\rightarrow$ M $-$ O)	6.30	Forbidden	141					
$4T_1$	$2t_2 \rightarrow 3t_2$ (O $\rightarrow$ M $-$ O)	6.34	Forbidden	141					
$3E$	$2t_2 \rightarrow 3t_2$ (O $\rightarrow$ M $-$ O)	6.38	Forbidden	141					
$4T_2$	$2t_2 \rightarrow 3t_2$ (O $\rightarrow$ M $-$ O)	6.90	$8.23 * 10^{-3}$	141	6.45	W	V	6.02[e]	5.57[e]

Region B									
$5T_1$	$1t_2 \rightarrow 2e$ (M + O → M − O)	8.15	Forbidden	142	7.69	Sh		7.28	5.66
$2A_2$	$1e \rightarrow 2e$ (M + O → M − O)	8.33	Forbidden	142					
$5T_2$	$1t_2 \rightarrow 2e$ (M + O → M − O)	8.42	$7.42 * 10^{-4}$	142	8.00	S	VI		
$4E$	$1e \rightarrow 2e$ (M + O → M − O)	8.56	Forbidden	142	8.31	Sh			
$6T_1$	$1t_1 \rightarrow 2a_1$ (O → M)	9.40	Forbidden	150	9.16	S			
$2A_1$	$1e \rightarrow 2e$ (M + O → M − O)	9.41	Forbidden	142					
$6T_2$	$1t_2 \rightarrow 3t_2$ (M + O → M − O)	9.68	$6.79 * 10^{-1}$	146	9.55	S			
					9.98	W			
					10.17	S			
Region C									
$7T_2$	$2t_2 \rightarrow 2a_1$ (O → M)	10.19	$1.59 * 10^{-1}$	149	10.29	S			
$7T_1$	$1e \rightarrow 3t_2$ (M + O → M − O)	10.59	Forbidden	143	10.66	S			
$8T_1$	$1t_1 \rightarrow 4t_2$ (O → O(R))	10.85	Forbidden	159	10.79	S			
$5E$	$1t_1 \rightarrow 4t_2$ (O → O(R))	10.88	Forbidden	161					
$3A_2$	$1t_1 \rightarrow 4t_2$ (O → O(R))	10.91	Forbidden	159					
$3A_1$	$1a_1 \rightarrow 2a_1$ (M → M)	10.92	Forbidden	150					
$8T_2$	$1e \rightarrow 3t_2$ (M + O → M − O)	10.96	$2.75 * 10^{-2}$	143	11.10	S			
$9T_2$	$1t_1 \rightarrow 4t_2$ (O → O(R))	11.04	$1.63 * 10^{-3}$	158					
$9T_1$	$1t_2 \rightarrow 3t_2$ (M + O → M − O)	11.22	Forbidden	142					
Average discrepancy		0.21							

O(R) refers to the Rydberg orbital of oxygen.

[a] Ref 7.

[b] Ref 8.

[c] Ref 9.

[d] Transition is $2t_2 \rightarrow 3t_2$.

[e] Transition is $1a_1 \rightarrow 3t_2$.

TABLE VI. Excitation energies of OsO_4 (in eV).

State	Main configuration	SAC-CI			Experimental[a]		
		Excitation energy	Oscillator strength	Second moment	Excitation energy	Strength	Band
Region A							
$1T_1$	$1t_1 \rightarrow 2e$ (O → M − O)	3.22	Forbidden	144			
$1T_2$	$1t_1 \rightarrow 2e$ (O → M − O)	3.90	$3.65 * 10^{-2}$	144	4.34	S	I
$2T_1$	$2t_2 \rightarrow 2e$ (O → M − O)	4.51	Forbidden	143			
$2T_2$	$2t_2 \rightarrow 2e$ (O → M − O)	5.46	$7.82 * 10^{-2}$	144	5.21	S	II
$1E$	$1a_1 \rightarrow 2e$ (M → M − O)	5.74	Forbidden	143			
$2E$	$1t_1 \rightarrow 3t_2$ (O → M − O)	6.13	Forbidden	144			
$3T_2$	$1t_1 \rightarrow 3t_2$ (O → M − O)	6.41	$2.21 * 10^{-2}$	144	5.95	W	III
$1A_2$	$1t_1 \rightarrow 3t_2$ (O → M − O)	6.45	Forbidden	144			
$3T_1$	$1t_1 \rightarrow 3t_2$ (O → M − O)	6.51	Forbidden	144	6.94	W	IV
$1A_1$	$2t_2 \rightarrow 3t_2$ (O → M − O)	7.58	Forbidden	144			
$4T_1$	$2t_2 \rightarrow 3t_2$ (O → M − O)	7.59	Forbidden	144			
$3E$	$2t_2 \rightarrow 3t_2$ (O → M − O)	7.64	Forbidden	144			
$4T_2$	$2t_2 \rightarrow 3t_2$ (O → M − O)	8.40	$2.87 * 10^{-2}$	144	7.94	S	V
					8.06	W	

Region B							
$5T_1$	$1t_2 \rightarrow 2e$	(M + O → M − O)	8.93	Forbidden	144	8.80	S	
$6T_1$	$1t_1 \rightarrow 2a_1$	(O → M)	9.12	Forbidden	154			
$1A_2$	$1e \rightarrow 2e$	(M + O → M − O)	9.25	Forbidden	144			
$5T_2$	$1t_2 \rightarrow 2e$	(M + O → M − O)	9.28	$9.1 * 10^{-4}$	144	9.18	S	VI
$4E$	$1e \rightarrow 2e$	(M + O → M − O)	9.46	Forbidden	144	9.55	W	
Region C								
$6T_2$	$1t_1 \rightarrow 4t_2$	(O → O(R))	10.00	$1.11 * 10^{-1}$	156	10.04	W	
$5E$	$1t_1 \rightarrow 4t_2$	(O → O(R))	10.35	Forbidden	163			
$2A_1$	$1e \rightarrow 2e$	(M + O → M − O)	10.37	Forbidden	145			
$7T_1$	$1t_1 \rightarrow 4t_2$	(O → O(R))	10.38	Forbidden	163			
$3A_2$	$1t_1 \rightarrow 4t_2$	(O → O(R))	10.39	Forbidden	162			
$7T_2$	$2t_2 \rightarrow 2a_1$	(O → M)	10.58	$3.24 * 10^{-1}$	154	10.61	S	
$8T_2$	$1t_1 \rightarrow 4t_2$	(O → O(R))	10.98	$5.12 * 10^{-2}$	160	10.79	S	
$3A_1$	$2t_2 \rightarrow 4t_2$	(O → O(R))	11.47	Forbidden	162			
$6E$	$1t_1 \rightarrow 5t_2$	(O → O(R))	11.52	Forbidden	165			
$8T_1$	$1t_1 \rightarrow 3e$	(O → O(R))	11.53	Forbidden	166	10.95	S	
$9T_2$	$1t_1 \rightarrow 5t_2$	(O → O(R))	11.60	$5.10 * 10^{-3}$	168	11.04	S	
Average discrepancy			0.29					

O(R) refers to the Rydberg orbital of oxygen.

[a] Ref 7.

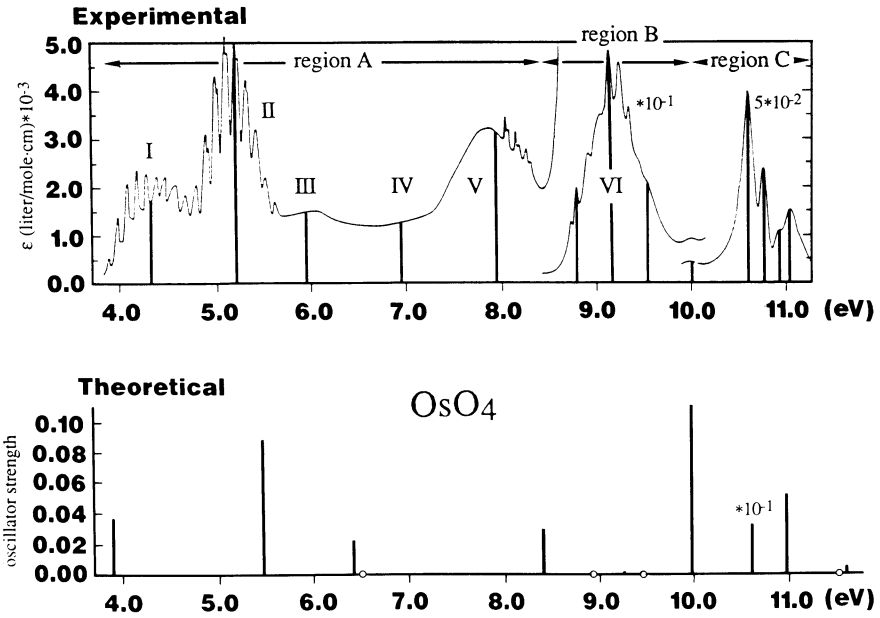

Figure 3. Experimental and theoretical electronic excitation spectra of OsO_4. Experimental spectra are cited from Ref. 7.

The transitions in region B, 9–10 eV, are characterized as excitations from the metal-oxygen bonding orbitals to the antibonding orbitals. The observed three peaks in this region, 8.80 eV (71,000 cm^{-1}), 9.18 eV (74,000 cm^{-1}), and 9.55 eV (77,000 cm^{-1}) are assigned to the $5T_1$ state [$1t_2$(M + O) → $2e$(M − O)], the $5T_2$ state [$1t_2$(M + O) → $2e$(M − O)], and the $4e$ state [$1e$(M + O) → $2e$(M − O)], respectively. The agreement between theory and experiment is very good for the excitation energy, though it is poor for the intensity. As noted for the region B spectra of RuO_4, the vibronic interaction, and the Jahn–Teller effect would be important for explaining the observed intensities of these high-symmetry transitions. The $6T_1$ state that is not assigned here to any peaks has a large second moment. This state is related to the $6T_1$ state of RuO_4.

Region C covers the peaks in 10–11 eV. We assign the peaks at 10.04 eV (81,000 cm^{-1}), 10.61 eV (85,600 cm^{-1}), 10.79 eV (87,000 cm^{-1}), 10.95 eV (88,300 cm^{-1}), and 11.04 eV (89,000 cm^{-1}) to the $6T_2$ state [$1t_1(2p(O)) \rightarrow 4t_2(3s(O))$], the $7T_2$ state [$2t_2(2p(O)) \rightarrow 2a_1(s(M))$], the $8T_2$ state [$1t_1(2p(O)) \rightarrow 4t_2(3s(O))$], and $8T_1$ state [$1t_1(2p(O)) \rightarrow 3e(3p(O))$], and the $9T_2$ state [$1t_1(2p(O)) \rightarrow 5t_2(3s(O))$], respectively. The $7T_2$, $8T_2$, $8T_1$, and $9T_2$ states of OsO_4 seem to correspond to the $7T_2$, $7T_1$, $8T_1$, and $8T_2$ states of RuO_4 from the shapes of the spectral peaks. The nature of these states are all Rydberg except for the $7T_2$ state, though only the $8T_1$ state is Rydberg in RuO_4. The peaks in region C generally correspond to the transitions from oxygen to metal and from oxygen $2p$ to the oxygen Rydberg orbitals. Foster et al. [7] considered that the Rydberg excitations of OsO_4 start

from 8.06 eV. The present results show, however, that the Rydberg excitations should be higher than about 10 eV, though the $6T_1$ state calculated at 9.12 eV has a relatively large second moment.

We see that in regions A and B, the excitation energies in OsO_4 are about 1.3 eV (theoretically about 1 eV) higher than the corresponding ones in RuO_4. The fact that the Os—O bond is stronger than is the Ru—O bond, as shown in Section 3.1, explains this difference between the transition energies of OsO_4 and RuO_4. The average discrepancy between the theoretical and experimental transition energies of OsO_4 is only 0.29 eV.

3.4. Ionized States

Table VII gives the experimental [10] and theoretical ionization energies and the intensities for RuO_4. The He-I photoelectron spectrum [10] and theoretical spectrum are displayed in Figure 4. The theoretical intensity is calculated by the monopole approximation in the final-state CI approximation [23],

$$I = \sum_{i}^{occ} \langle \Psi^{\text{SAC-CI}}(N-1) | a_i \Psi^{\text{HF}}(N) \rangle^2,$$

where I is intensity; a_i, the annihilation operator for the orbital ϕ_i; and $\Psi^{\text{SAC-CI}} \times (N-1)$ and $\Psi^{\text{HF}}(N)$, the SAC-CI wave function for the ionized state and the HF wave function for the neutral ground state, respectively. Table VII shows that Koopmans' approximation gives a wrong ordering as seen from the results of SAC-CI. Moreover, the theoretical intensities show that the effect of the final-state correlation is large, especially for the $1e$ and $1t_2$ ionizations. Thus, the electron correlations are very important in the ionized states. The first three peaks are assigned to ionizations from the outer-valence orbitals, $1t_1$, $2t_2$, and $1a_1$, respectively, and are in very good agreement with the experimental values. The present assignments are the same as those of the DVM-Xα method [8], but the SCF-Xα method [9] has given the same ordering as Koopmans' approximation.

The monopole approximation is not the very good description of the intensity of an ionization peak. However, the monopole intensity gives a measure to understand whether the ionization is due to the one-electron process or the two-electron process, such as the simultaneous ionization-excitation process. The first three ionizations are essentially attributed to the one-electron process, though the theoretical intensities are less than 0.9 even in this outer-valence region. The band higher than 15 eV in the experimental spectrum is broad and shows more complicated features. The present calculations indicate that this broad band consists of two ionizations mainly from the $1e$ and $1t_2$ MOs, though the agreement between theory and experiment is not good enough in this case. The intensities of these ionizations are less than 0.8, showing that the two-electron processes strongly mix with the single ionizations. Further, several satellite lines due to the shake-up ionizations are calculated in the higher-energy region of the $1t_2$ ionization energy. The asymmetry of the band D is understood as

TABLE VII. Ionization energies (eV) and intensities of RuO_4.

Ionization				SAC-CI				
State	Orbital picture	Nature	Koopmans'	*Ip*	Intensity	Experimental[a]	DVM-Xα[b]	SCF-Xα[c]
1^2T_1	$1t_1 \rightarrow \infty$	$O \rightarrow \infty$	14.67	12.11	0.87	12.15	11.96	14.4
1^2T_2	$2t_2 \rightarrow \infty$	$O \rightarrow \infty$	15.65	12.93	0.87	12.92	12.92	14.8
1^2A_1	$1a_1 \rightarrow \infty$	$M \rightarrow \infty$	15.46	13.68	0.88	13.93	13.49	14.7
1^2E	$1e \rightarrow \infty$	$M + O \rightarrow \infty$	21.11	17.66	0.71	16.4	16.41	17.5
2^2T_2	$1t_2 \rightarrow \infty$	$M + O \rightarrow \infty$	20.87	17.77	0.79		16.45	18.0
1^2A_2	$(1t_1)^2 \rightarrow (2e, \infty)$	$O, O \rightarrow M - O, \infty$		18.09	0.006			
2^2E	$(1t_1)^2 \rightarrow (2e, \infty)$	$O, O \rightarrow M - O, \infty$		18.30	0.04			
2^2A_1	$(1t_1)^2 \rightarrow (2e, \infty)$	$O, O \rightarrow M - O, \infty$		18.36	0.004			

[a] Ref 10.
[b] Ref 8.
[c] Ref 9.

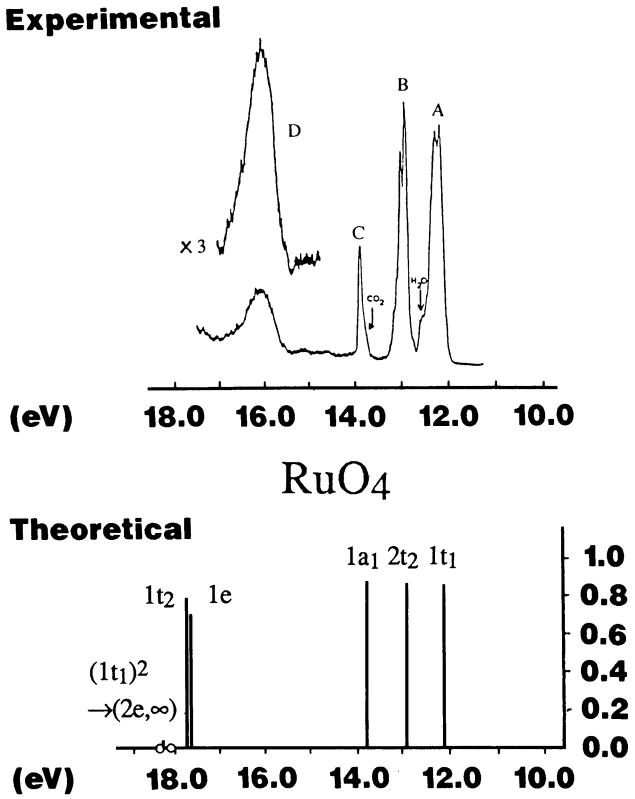

Figure 4. Experimental and theoretical ionization spectra of RuO_4. Experimental spectra are cited from Ref. 10.

the existence of these satellites. It should be noted that these shake-up processes involve an electron transfer from oxygen to metal.

Table VIII gives the experimental [10] and theoretical ionization energies and theoretical intensities for OsO_4. Figure 5 shows the experimental [10] and theoretical spectra. Again, Koopmans' ordering of the inner-valence orbitals, $1e$ and $1t_2$, differs from the ordering of SAC-CI. The effects of electron correlations are important as in RuO_4. The theoretical intensities of OsO_4 are less than 0.9 similarly to RuO_4. The ionization energies of the $1t_1$ and $2t_2$ MOs are almost the same as those of RuO_4, because these orbitals are almost the nonbonding $2p$ orbitals of the oxygen ligands. In the experimental spectrum of OsO_4, a peak, denoted as C in Figure 5, is present at 13.14 eV but there is no corresponding peak in the RuO_4 spectrum. Diemann and Müller gave two possible explanations for this peak [24]. One is that this peak is due to the ionization from the orbital different from the other peaks. Another is that the peak C splits out from the peak B by the vibronic Jahn–Teller effect or by the spin-orbit coupling in the ionic $^2T_2$ state. The present calculations do not support the former explanation, and so the second one may be a plausible orgin. Peaks D and E are similar to those of

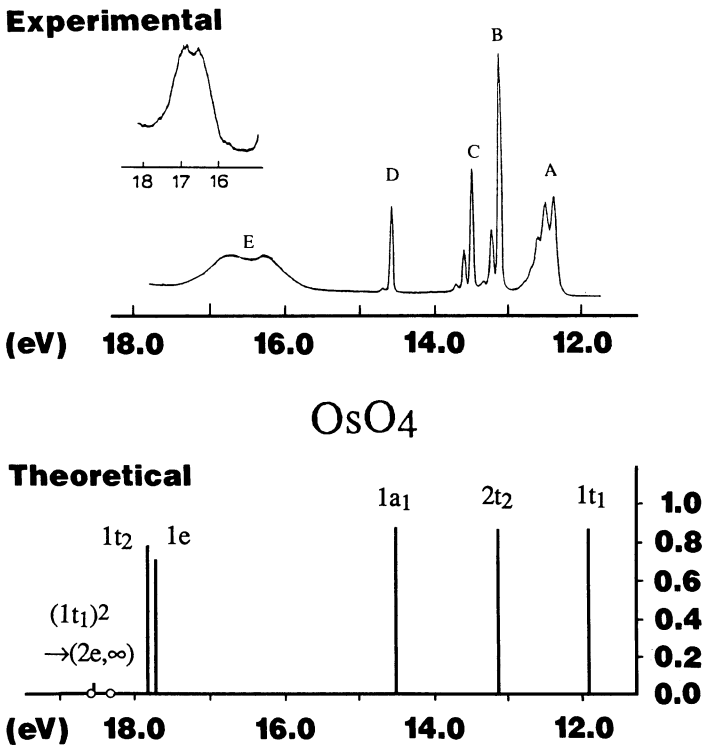

Figure 5. Experimental and theoretical ionization spectra of OsO_4. Experimental spectra are cited from Ref. 10.

RuO_4, but the ionization energies of these peaks are larger than those of RuO_4, since the Os—O bond is stronger than is the Ru—O bond as examined in Section 3.1. The electron-transfer shake-up peaks follow the $1t_2$ ionization similarly to the case of RuO_4. Evans et al. found out a general rule from a series of the studies on the photoelectron spectra of $Mn(CO)_5$ derivatives [25]: that the photoelectron spectra are divided into three regions in the order of increasing ionization energy as the ionizations from (1) metal *d*-orbitals, (2) bonding orbitals between metal and ligand, and (3) pure ligand orbitals. For RuO_4 and OsO_4, the ionization spectra are classified as the ionizations from the ligand orbitals, the metal *s*-orbital, and the bonding orbitals between metal and oxygen in the order of increasing energy.

4. Conclusion

We have applied the SAC and SAC-CI theories to the calculation of the excited and ionized states of RuO_4 and OsO_4. We have tried to clarify the whole range of the observed spectra by the ab initio theories including electron correlations.

For the ground state of these complexes, electron correlations work to relax the charge polarization of the M—O bonds. It is shown that the Os—O bond is

TABLE VIII. Ionization energies (eV) and intensities of OsO_4.

Ionization				SAC-CI		
State	Orbital picture	Nature	Koopmans'	*Ip*	Intensity	Experimental[a]
1^2T_1	$1t_1 \rightarrow \infty$	$O \rightarrow \infty$	12.57	11.93	0.87	12.35
1^2T_2	$2t_2 \rightarrow \infty$	$O \rightarrow \infty$	15.87	13.14	0.87	13.14
						13.54
1^2A_1	$1a_1 \rightarrow \infty$	$M \rightarrow \infty$	16.50	14.54	0.88	14.66
1^2E	$1e \rightarrow \infty$	$M + O \rightarrow \infty$	21.11	17.74	0.71	16.4
2^2T_2	$1t_2 \rightarrow \infty$	$M + O \rightarrow \infty$	20.67	17.85	0.79	16.8
1^2A_2	$(1t_1)^2 \rightarrow (2e, \infty)$	$O, O \rightarrow M - O, \infty$		18.35	0.005	
2^2E	$(1t_1)^2 \rightarrow (2e, \infty)$	$O, O \rightarrow M - O, \infty$		18.57	0.06	
2^2A_1	$(1t_1)^2 \rightarrow (2e, \infty)$	$O, O \rightarrow M - O, \infty$		18.59	0.004	

[a] Ref 10.

stronger than is the Ru—O bond. This difference in bond is understood from the atomic-energy levels of the Ru, Os, and oxygen atoms. It explains the differences in the transition energies and the ionization energies of RuO_4 and OsO_4.

The excitation spectra of RuO_4 and OsO_4 are conveniently divided into three regions. The transitions in region *A* are from the nonbonding orbitals of oxygen to the antibonding orbitals between metal and oxygen. Those in region *B* are from the bonding orbitals between metal and oxygen to the corresponding antibonding orbitals. Those in region *C* are from oxygen to metal ($7T_2$) and the Rydberg excitations within the oxygen ligands. The fact that the transition energies of OsO_4 in regions *A* and *B* are larger than those of RuO_4 is understood from the difference in the strength of the M—O bonds.

For the outer-valence ionizations, the present results are in good agreement with the experimental data. The shake-up configurations mix with the one-electron processes in the inner-valence regions. Koopmans' approximation gives the incorrect ordering of the ionization energies. The shake-up satellite peaks appear in the higher-energy region of the one-electron ionization processes. They involve the electron-transfer from oxygen to metal. In the OsO_4 spectrum, peak *C* is probably due to the vibronic Jahn–Teller effect or the spin-orbit coupling in the ionic $^2T_2$ state.

After the submission of this manuscript, the referee kindly let us know the existence of a study on RuO_4 studied by the RHF and CI methods [26], which we could not know before.

5. Acknowledgments

We would like to thank Dr. O. Kitao for some helpful advice in the computations. The calculations were carried out on the FACOM M780 computer at the Data Processing Center of Kyoto University and the HITAC M680H and S820/80 computers at the Institute for Molecular Science. This study has partially been supported by the Grant-in-Aids for Scientific Research from the Ministry of Education, Science and Culture of Japan.

Bibliography

[1] H. Nakatsuji and K. Hirao, J. Chem. Phys. **68**, 2053 (1978).
[2] H. Nakatsuji, Chem. Phys. Lett. **59**, 362 (1978); **67**, 329 (1979).
[3] H. Johansen and S. Rettrup, Chem. Phys. **74**, 77 (1983).
[4] I. H. Hillier and V. R. Saunders, Proc. Roy. Soc. Lond. **A320**, 161 (1970); I. H. Hillier and V. R. Saunders, Chem. Phys. Lett. **9**, 219 (1971); P. D. Dacre and M. Elder, Chem. Phys. Lett. **11**, 377 (1971); H. Johansen, Chem. Phys. Lett. **17**, 569 (1972); J. A. Connor, I. H. Hillier, V. R. Saunders, W. H. Wood, and M. Barder, Mol. Phys. **24**, 497 (1972).
[5] K. H. Johnson and F. C. Smith, Jr, Chem. Phys. Lett. **10**, 219 (1971); T. Sasaki and H. Adachi, J. Electron Spectrosc. Relat. Phenom. **19**, 261 (1980); A. Golebiewski and M. Witko, Acta Phys. Pol. **A57**, 585 (1980).
[6] H. Nakatsuji, Int. J. Quantum Chem., Quantum Chem. Symp. **17**, 241 (1983).
[7] S. Foster, S. Felps, L.W. Johnson, D. B. Larson, and S. P. McGlynn, J. Am. Chem. Soc. **95**, 6578 (1973).
[8] T. Ziegler, A. Rauk, and E. J. Baerends, Chem. Phys. **16**, 209 (1976).

[9] A. Gupta and J. A. Tossell, J. Electron Spectrosc. Relat. Phenom. **26**, 223 (1982).
[10] P. Burroughs, S. Evans, A. Hamnett, A. F. Orchard, and N.V. Richardson, J. Chem. Soc. Faraday Trans. 2 **70**, 1895 (1974).
[11] B. Krebs and K. D. Hasse, Acta Crystallograph. **B32**, 1334 (1976).
[12] P. J. Hay and W. R. Wadt, J. Chem. Phys. **82**, 270 (1985).
[13] S. Huzinaga, *Gaussian Basis Sets for Molecular Calculation* (Elsevier, Amsterdam, 1984).
[14] H. F. Schaefer, *Methods of Electronic Structure Theory* (Plenum, New York, 1977).
[15] B. R. Brooks, P. Saxe, W. D. Laidig, and M. Dupuis, Program System GAMESS; Program Library No. 481, Computer Center of the Institute for Molecular Science, (1981).
[16] H. Nakatsuji, Program System for SAC and SAC-CI calculations, Program Library No. 146 (Y4/SAC), Data Processing Center of Kyoto University (1985); Program Library SAC85, No. 1396, Computer Center of the Institute for Molecular Science (1986).
[17] H. Nakatsuji , Chem. Phys. **75**, 425 (1983).
[18] M. Krauss and W. J. Stevens, J. Chem. Phys. **82**, 5584 (1985).
[19] C. E. Moore, *Atomic Energy Levels* (National Bureau of Standards, Washington, DC, 1971).
[20] A. Müller and E. Diemann, MTP Int. Rev. Sci., Inorg. Chem. Ser. II, (Butterworth, London, 1974), Vol. 5, p. 71.
[21] H. Nakatsuji , K. Kanda, K. Endo, and T. Yonezawa, J. Am. Chem. Soc. **106**, 4653 (1984).
[22] H. Johansen, Mol. Phys. **49**, 1209 (1976).
[23] R. L. Martin and D. A. Shirley, J. Chem. Phys. **64**, 3685 (1976).
[24] E. Diemann and A. Müller, Chem. Phys. Lett. **19**, 538 (1973).
[25] S. Evans, J. C. Green, M. L. H. Green, A. F. Orchard, and D.W. Turner, Discuss. Faraday Soc. **47**, 112 (1969).
[26] M. Lenz, Thesis submitted to the Technical University of Denmark, entitled "Electronic Structure and Spectra of Selected 1. and 2. Row Transition Metal Tetraoxy Complexes" (in Danish) (1983).

Received August 14, 1989
Accepted for publication December 29, 1989